catalysts

MDPI

Article

Comprehensive Kinetics of the Photocatalytic Degradation of Emerging Pollutants in a LED-Assisted Photoreactor. S-Metolachlor as Case Study

Laura Rancaño [1], Maria J. Rivero [1], Miguel Ángel Mueses [2] and Inmaculada Ortiz [1,*]

[1] Department of Chemical and Biomolecular Engineering, Avenida Los Castros s/n, 39100 Santander, Spain; laura.rancano@unican.es (L.R.); mariajose.rivero@unican.es (M.J.R.)
[2] Modelling and Application of Advanced Oxidation Processes, Photocatalysis and Solar Photoreactors Engineering, Chemical Engineering Program, University of Cartagena, Postal 195, Cartagena 1382, Colombia; mmueses@unicartagena.edu.co
* Correspondence: Inmaculada.ortiz@unican.es; Tel.: +34-942-201585

Abstract: Although the potential and beneficial characteristics of photocatalysis in the degradation of a good number of emerging pollutants have been widely studied and demonstrated, process design and scale-up are restrained by the lack of comprehensive models that correctly describe the performance of photocatalytic reactors. Together with the kinetics of degradation reactions, the distribution of the radiation field in heterogeneous photocatalytic systems is essential to the optimum design of the technology. Both the Local Volumetric Rate of Photon Absorption (LVRPA) and the Overall Volumetric Rate of Photon Absorption (OVRPA) help to understand this purpose. This work develops a Six-Flux radiation absorption–scattering model coupled to the Henyey–Greenstein scattering phase function to evaluate the LVRPA profile in a LED-assisted photocatalytic reactor. Moreover, the OVRPA has been calculated and integrated into the kinetic equation, accounting for the influence of the radiation distribution on the reaction rate. The model has been validated with experimental data for the degradation of S-Metolachlor (MTLC), and the set of operating variables that maximize the reactor performance, 0.5 g/L of TiO_2 P25 and pH 3, has been determined.

Keywords: heterogeneous photocatalysis; S-Metolachlor; radiation distribution; kinetic modeling

Citation: Rancaño, L.; Rivero, M.J.; Mueses, M.Á.; Ortiz, I. Comprehensive Kinetics of the Photocatalytic Degradation of Emerging Pollutants in a LED-Assisted Photoreactor. S-Metolachlor as Case Study. *Catalysts* **2021**, *11*, 48. https://doi.org/10.3390/catal11010048

Received: 30 November 2020
Accepted: 30 December 2020
Published: 31 December 2020

1. Introduction

Worldwide population growth has resulted in increasing food demands; as a consequence, the use of herbicides and pesticides has increased in recent years. One of the pesticides most frequently used to control the expansion of grassy weeds is S-Metolachlor (MTLC). Considering the relatively low soil/water partitioning of S-Metolachlor, it is expected to be moderately to highly mobile in soil. Therefore, substantial leaching by run-off is expected to occur. Due to its solubility and slow biological degradation rate, its presence in natural waters persists after long periods, and it has even been detected in drinking water [1]. A concentration of 5.37 μg/L of S-Metolachor was detected in Spanish groundwater [2]. It was also found in surface water in the concentration range from 0.1 to 10 μg/L [3]. Cavalier et al. [4] reported concentrations in the range from 1 to 5 μg/L for MTLC in Arkansas' groundwaters. The National Water-Quality Assessment (NWQA) program reported that S-Metolachlor was detected in representative watersheds and aquifers in concentrations below 0.013 μg/L between 1992 and 2001 in the United States [5]. Moreover, the European Union included in the EU directive 2006/118/EC a limit of 0.1 μg/L for the concentration of this type of pesticide in groundwaters. The Spanish national directive Real Decreto 817/2015 published a priority substances list with 16 compounds, including S-Metolachlor with a maximum admissible value of 1 μg/L in continental surface waters [6].

S-Metolachlor belongs to the chloroacetamides group. Its lifetime in acidic water is 200 days and 97 days in basic water. It can be extremely toxic to aquatic biodiversity and has been classified as a carcinogenic compound [3]. Degradation of MTLC by conventional treatments such as physical adsorption [7], coagulation, chlorination or biological [8] and bio-electrochemical [9] treatments has been studied, but these technologies report a low yield. Therefore, high-performance and low-cost processes such as Advanced Oxidation Processes (AOPs) are sought for the efficient degradation of this pesticide [3,10–16].

Among AOPs, heterogeneous photocatalysis is effective for the removal of many recalcitrant organic contaminants from polluted waters [3,10–16]. One of its main advantages is that solar light can activate the catalyst. However, some challenges remain unsolved to improve the overall photocatalytic process efficiency. Recently, the use of ultraviolet Light-Emitting Diodes (LEDs) as a light source in photocatalytic processes has received increasing attention due to their high efficiency and stability [13,14,17,18]. Thus, modeling the radiation field and the spatial distribution of the radiation absorption inside LED-assisted photocatalytic reactors is a scientific challenge that can contribute to the further development of the technology [19–23].

Regarding the modeling of heterogeneous photocatalytic reactors, the irradiance distribution inside the reactor can be described with the rigorous solution of the Radiative Transfer Equation (RTE), detailed in the Supplementary Materials [19,23,24]. Romero et al. [25] reported the radiation field modeling in an annular photocatalytic reactor based on a system of differential equations. However, the model involved high resolution complexity [22]. To solve the set of model equations, the Discrete Ordinate Method (DOM) and the Photon Monte Carlo algorithm (PMC) were the most commonly used methods when no simplifications could be assumed [26]. Some authors reported the solution of the RTE by estimation of the Local Volumetric Rate of Photon Absorption (LVRPA) using different mathematical approximations that made the numerical resolution of the equations easier [27,28]. A somewhat simpler approach to estimate the radiation field comprised the application of the Six-Flux Absorption–Scattering Model to the Henyey–Greenstein scattering phase function (SFM-HG) based on the assumption that in a heterogeneous photocatalytic reactor the scattering of photons occurs only along the six Cartesian directions, which is described in the Supplementary Materials [22]. The SFM algebraic nature required short computational times and low mathematical complexity [21]. This model was used by Mueses et al. [29] to analyze the effective radiation in a Compound Parabolic Collector photocatalytic reactor (CPC). Later, Ochoa-Gutiérrez et al. [30] used the same model to simulate the solar radiation field in an Offset Multitubular Photoreactor (OMTP). Martín-Sómer et al. [31] focused their efforts on evaluating the influence of the light distribution in an annular reactor provided with either Hg lamps or LEDs using Computational Fluid Dynamics (CFD). Furthermore, Casado et al. [18] contributed to the design of annular photocatalytic reactors with CFD simulation and optimization of the LEDs location in the reactor, and Moreno et al. [26] reported the improvement of the DOM resolution method for LED light source simulations.

Regarding the degradation kinetics, most previous photocatalytic studies proposed pseudo-first-order kinetic equations to describe the degradation rate of the target species, thus the influence of radiation absorption by the catalyst was lumped in the kinetic constant. Therefore, developing a kinetics expression that disaggregates the reaction kinetics parameters from the radiation parameters becomes necessary to advance the reactor design [12–14,16,32–35].

Accordingly, the objective of this work is to develop a comprehensive model to describe the degradation kinetics of emerging pollutants in a UV-LED photoreactor by incorporating the radiation distribution inside the reactor for a proper description of the influence of operation variables and parameters. To this end, the radiation field has been described using the RTE equation, and the LVRPA has been calculated using the SFM-HG model. Finally, a kinetic model that includes the radiation influence using the OVRPA has been developed. The proposed model has been validated for the removal of the herbicide MTLC in a UV-LED reactor.

2. Results and Discussion

First, MTLC dark absorption on the surface of TiO_2 was assessed, and the results confirmed that after 30 min it was negligible. No degradation by photolysis was observed for a LED irradiance of 22.65 mW/cm^2, which corresponded to an electrical consumption of 50 W. This irradiance value was used for further experiments.

2.1. Influence of the Experimental Variables

In photocatalytic processes, pH is a crucial variable since it can modify the rate of degradation of the target compound due to changes in the catalyst surface [36]. Three pH values were evaluated. It can be observed in Figure 1 that natural pH and basic pH provided similar results in MTLC removal. Faster elimination was obtained at pH values below the isoelectric point of TiO_2 (pH = 6.5) [12]. The positive charge of the catalyst surface at these conditions facilitated the photodegradation of methyl groups and the hydroxylation of the aromatic ring [36,37]. Figure 2 shows a comparison between the initial and final pH values. A higher reduction in the concentration of MTLC was observed at pH 3. Valencia et al. [38] also reported the best photocatalytic degradation of similar herbicides at acidic conditions. Starting at natural pH, the pH decreased by 1.02 units. Sakkas et al. [10] and Guelfi et al. [11] attributed the decrease of pH at natural pH conditions to the formation of organic acids during MTLC degradation. Acidic conditions were concluded to be the most beneficial for herbicide removal [39,40]. Therefore, the rest of the photocatalytic experiments were carried out at pH 3.

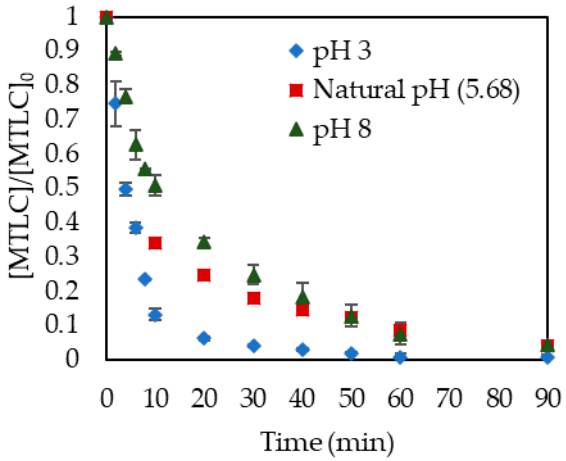

Figure 1. pH influence on S-Metolachlor degradation. Catalyst concentration: 0.5 g/L.

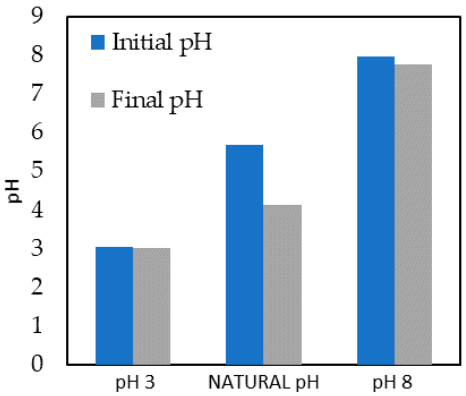

Figure 2. Comparison of initial and final pH after 480 min.

Figure 3 shows that the rate of MTLC removal increased with the catalyst concentration in the range between 0.05 g/L and 0.5 g/L of TiO_2 P25. Under these conditions, total MTLC elimination was achieved after 40 min of treatment. For catalyst concentrations above 0.5 g/L. a negative influence of this variable on the degradation rate was observed. This was attributed to the light shield phenomena exerted by the catalyst. The experiments were carried out in duplicate. Results showed an average standard deviation of 2%.

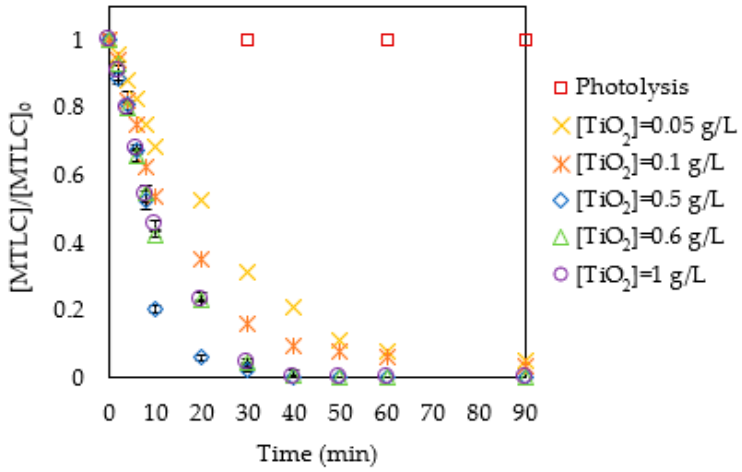

Figure 3. Dimensionless S-Metolachlor (MTLC) concentration removal at pH 3.

Figure 4 shows the chloride concentration during several photocatalytic experiments and the theoretical chloride released from the MTLC molecule. The theoretical chloride released was calculated by a mass balance, assuming that for each mole of MTLC removed, one mole of Cl^- was released to the reaction media. It can be observed that as long as MTLC is removed, chloride ions appear in the solution. The release of chloride ions slows down when the catalyst concentration is higher than 0.6 g/L, which is in agreement with the trend in MTLC degradation. As shown in Figure 3, for catalyst concentrations higher than 0.6 g/L, the degradation rate slowed down. Nevertheless, the concentration of chloride ions in the solution is less than the calculated value corresponding to the degradation of the MTLC molecule. This is explained by the formation of organochlorinated intermediates that remain in the solution during the first minutes. The degradation route has been previously reported [10,11]. Guelfi et al. [11] identified by-products by GC-MS and found two groups: chlorinated and nonchlorinated compounds. The first group appeared when the OH^-·radicals attacked the aromatic ring, and the group $–COCH_2Cl$ remained in the molecule leading to chlorinated intermediates such as chloroacetic acid. The second group of compounds was formed from the release of the Cl^- atoms. In all cases, after 180 min the total amount of released chloride corresponds to the atoms in the original MTLC molecule. Moreover, when the catalyst concentration was 0.5 g/L, chloride was completely released in 120 min.

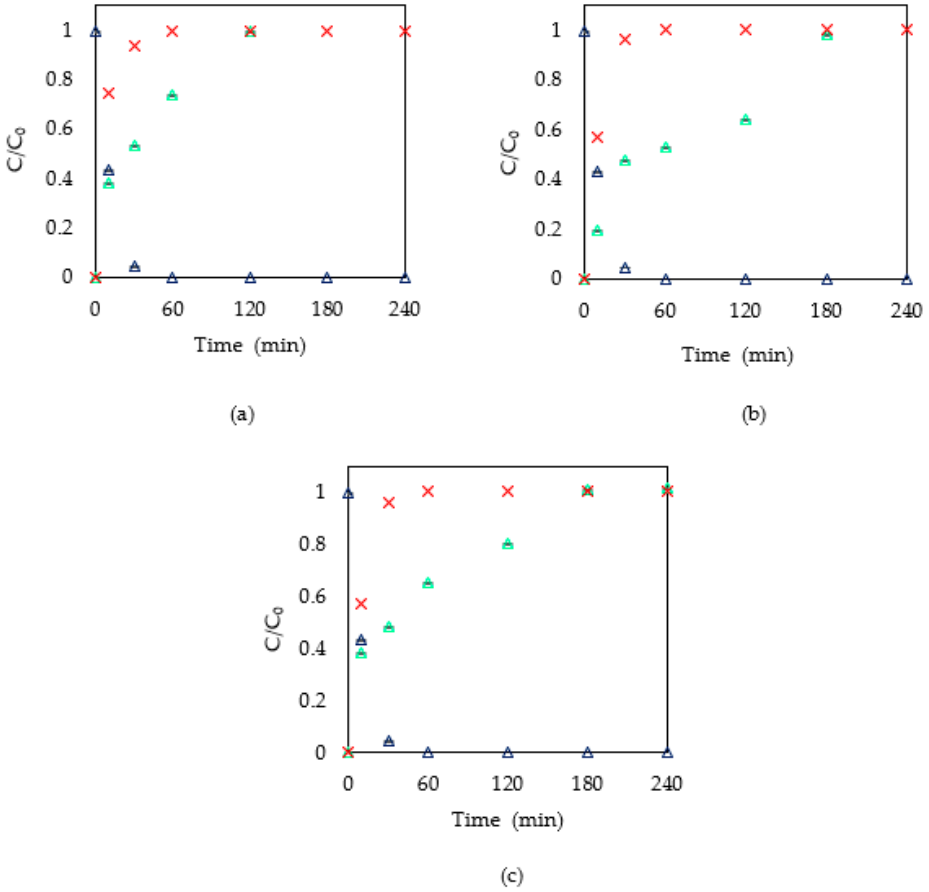

Figure 4. Chloride ions in solution (**a**) 0.5 g/L of TiO_2, (**b**) 0.6 g/L of TiO_2, (**c**) 1 g/L of TiO_2. Δ MTLC removal, Δ chloride ions released during MTLC removal, X chloride concentration corresponding to the theoretical chloride release from the MTLC molecule.

2.2. Radiation Modeling

The proposed model for LVRPA evaluation provides the photonic absorption profiles corresponding to different catalyst concentrations, as depicted in Figure 5. It is remarkable that when the catalyst concentration increases, so does the maximum value of LVRPA. It can be concluded that the increase of the catalyst concentration enhances the photonic absorption in the reactor wall (0 m) but has the opposite effect inside the reactor until the minimum value is reached in the center of the reactor (0.04 m). The decrease in the inner part of the reactor is due to the shielding effect of the catalyst particles [41]. The same trend was observed by Moreno-San Segundo et al. [42] when modeling an annular LED photoreactor.

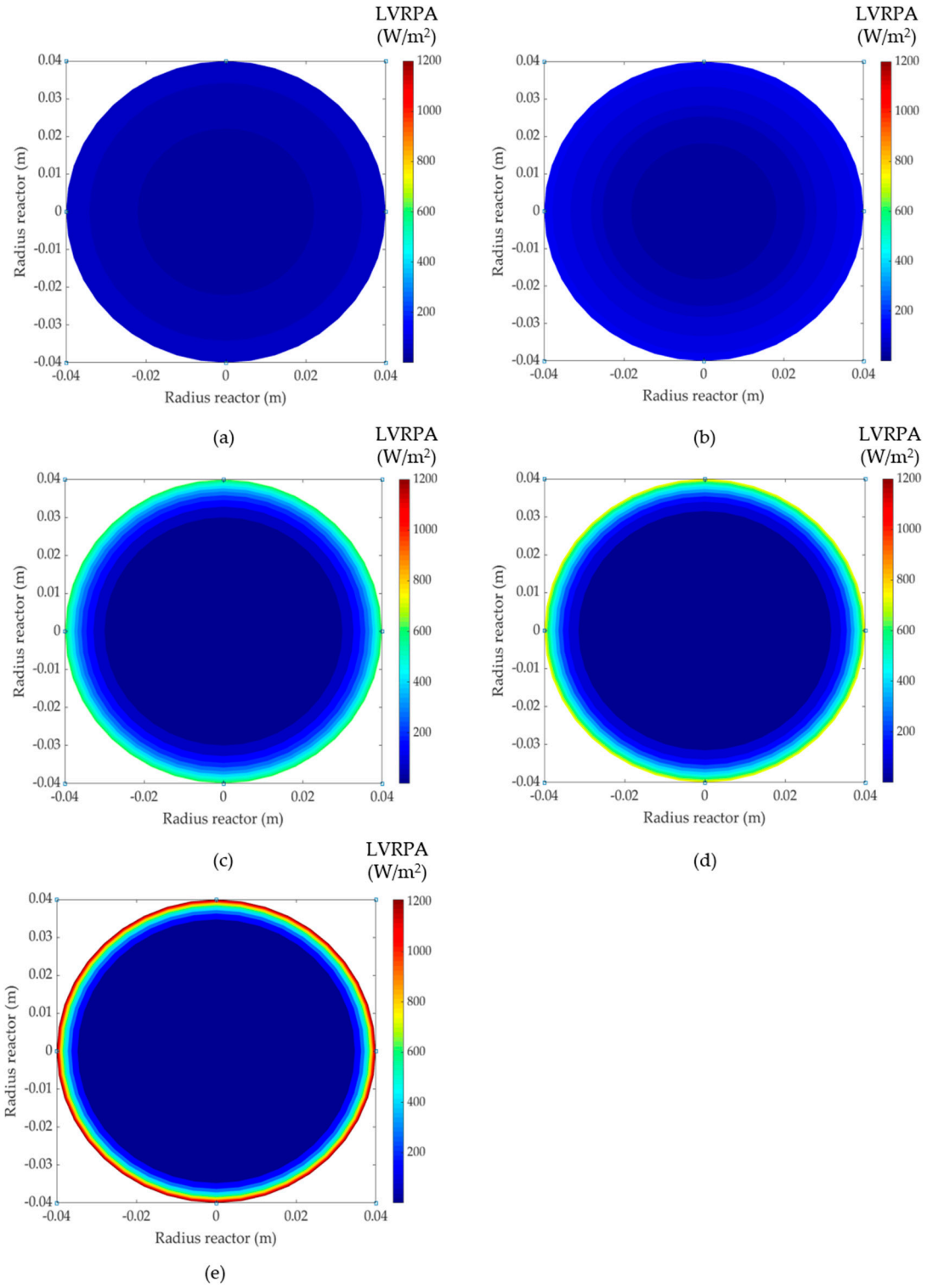

Figure 5. Simulated Local Volumetric Rate of Photon Absorption (LVRPA) values in the reactor for (**a**) 0.05 g/L TiO_2, (**b**) 0.1 g/L TiO_2, (**c**) 0.5 g/L TiO_2, (**d**) 0.6 g/L TiO_2 and (**e**) 1.0 g/L TiO_2.

Moreover, the LVRPA profiles that describe the radiation field in solar parabolic collectors applying the SFM model have been previously reported by Colina-Márquez et al. [37] and Mueses et al. [29]. In that case, the model results showed that the maximum LVRPA value was achieved on the illuminated area of the reactors, but the radiation profiles were not symmetrical because the reactors were not homogeneously illuminated. In the present

work, the LED light sources were placed surrounding the reactor, therefore the adsorption of the radiation was enhanced. Accordingly, the higher the photon absorption area, the higher the probability the photocatalytic reaction occurs.

LVRPA profiles inside the reactor were integrated for the total reaction volume in order to obtain the Overall Volumetric Rate of Photon Absorption (OVRPA), which is useful to optimize the catalyst concentration. Figure 6 shows that when the catalyst concentration increases, so does OVPRA until the maximum value is obtained for a catalyst concentration of 0.5 g/L. For concentrations higher than this value, OVRPA is kept almost constant. This result agrees with the influence of the catalyst concentration on the MTLC degradation rate that has been experimentally observed. A similar dependency of OVRPA with catalyst concentration has been reported for different systems by Acosta-Herazo et al. [19], Casado et al. [41], Colina-Márquez et al. [37], Marugán et al. [20] and Tolosana-Moranchel [43,44].

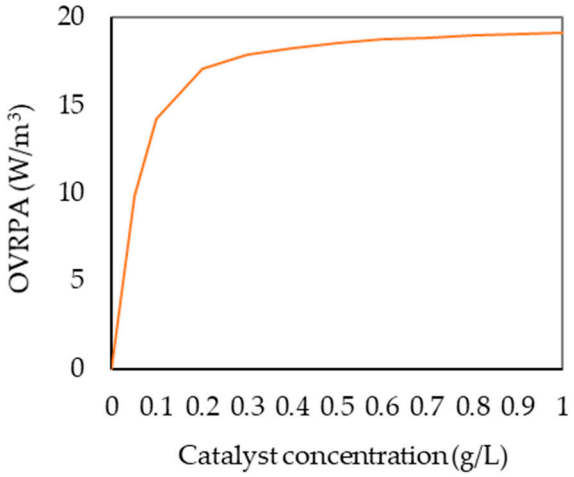

Figure 6. Influence of the catalyst concentration on Overall Volumetric Rate of Photon Absorption (OVRPA).

Therefore, this methodology confirms the influence of catalyst concentration on radiation absorption and constitutes a useful tool to describe the light availability inside the reactor.

2.3. Kinetic Modeling

Equation (1) has been used to describe the rate of photocatalytic degradation of MTLC.

$$-r_A = \frac{dC_A}{dt} = k \times (OVRPA)^m \times {C_A}^n \quad (1)$$

where C_A is the concentration of MTLC, k the kinetic constant and OVRPA is the overall volumetric rate of photon absorption in the photocatalytic reactor. In this equation, the OVRPA was included in the kinetic model to consider the influence of the radiation distribution on the reaction rate. The OVRPA values corresponding to different concentrations of TiO_2 are shown in Table 1. The values of m and n parameters represent the dependence of the reaction rate of a substrate on OVRPA and on the substrate concentration, respectively. The value of m should be in the range between 0.5 and 1. As m increases, the model becomes more sensitive to changes in the incident radiation [19,23]. In this work, the set of parameters m, n and k has been estimated from the fitting of simulated to experimental data using the Aspen Custom Modeler software (Aspentech).

Table 1. OVRPA values for the photocatalytic experiments.

[TiO_2 P25] (g/L)	OVRPA (W/m^3)
0.05	9.80
0.1	14.24
0.5	18.54

In order to determine the set of values of the parameters m, n and k that best fit the experimental results the minimum value of the weight standard deviation, as defined in Equation (2), was used as the criterion.

$$\sigma = \sqrt{\frac{\sum_{i=1}^{N}\left(\frac{C_{exp}-C_{sim}}{C_{exp}}\right)^2}{N-1}} \quad (2)$$

In Table 2, it can be observed that the lowest values of standard deviation were obtained for n = 1 and 0.8 < m < 1.0 so that further optimization in a narrower range provided the best fitting for the set of parameters m = 0.9 and n = 1.1 (Figure 7) with a standard deviation of 0.31. The kinetic constant for the optimal case was 5.1×10^{-3} $(m^3)^{0.9}/W^{0.9}\cdot min\cdot mol^{0.1}$.

Table 2. Kinetic constants and standard deviations for different sets of m and n parameters.

	n = 0.5			**n = 1**		
	m = 0.5	m = 0.8	m = 1	m = 0.5	m = 0.8	m = 1
$\left[\frac{k}{\frac{min\cdot(m^3)^{(m+n)-1}}{(W)^m\cdot(mol)^{n-1}}}\right]$	7.2×10^{-2}	3.2×10^{-2}	2.0×10^{-2}	1.5×10^{-2}	6.0×10^{-3}	3.9×10^{-3}
σ	0.72	0.65	0.59	0.43	0.39	0.39
	n = 1.5			**n = 2**		
	m = 0.5	m = 0.8	m = 1	m = 0.5	m = 0.8	m = 1
$\left[\frac{k}{\frac{min\cdot(m^3)^{(m+n)-1}}{(W)^m\cdot(mol)^{n-1}}}\right]$	8.5×10^{-3}	3.4×10^{-3}	1.7×10^{-3}	2.5×10^{-3}	1.4×10^{-3}	7.0×10^{-4}
σ	0.55	0.51	0.48	0.63	0.56	0.55

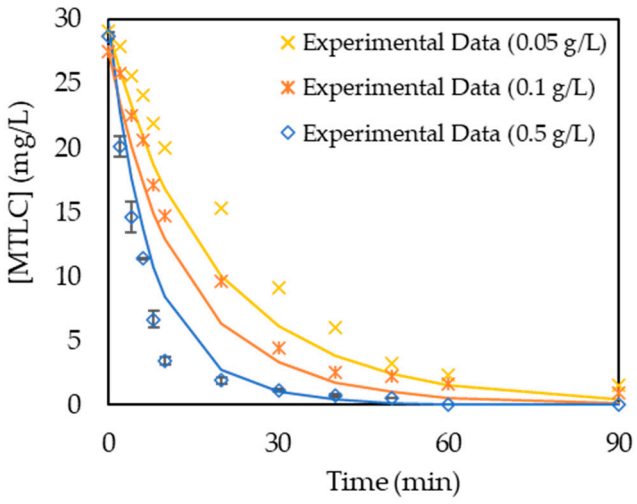

Figure 7. Kinetic model validation for m = 0.9 and n = 1.1. Continuous lines correspond to model simulations.

The value of m is related to the dependence of the degradation kinetics of the target organic compound on light radiation. Fractional values of m have been previously reported for the photocatalytic degradation of isoproturon in an annular photocatalytic reactor, where values of m = 0.82 and n = 1.0 corresponded to the best fitting to experimental data [23].

3. Materials and Methods

3.1. Chemicals

MTLC PESTANAL Analytical Standard, sulfuric acid 98% (H_2SO_4) and sodium hydroxide (NaOH) were obtained from Sigma-Aldrich (Merck KGaA, Darmstadt, Germany). Titanium dioxide catalyst (TiO_2) Aeroxide P25 was purchased from Evonik Industries (Essen, Germany) and acetonitrile gradient grade (C_2H_3N), methanol (CH_3OH), oxalic acid ($C_2H_2O_4$) and iron chloride ($FeCl_3$) were purchased from PANREAC (Barcelona, Spain). Perchloric acid ($HCLO_4$) was obtained from Scharlau (Barcelona, Spain).

3.2. Experimental Methodology for the Photocatalytic Experiments

The photoreactor (Figure 8) was purposely designed for this work. It was composed of a control panel, which provides temperature, intensity and electrical power information (1). The samples were collected from the reactor through a sample pipe (2). The reaction medium was homogenized by magnetic stirring (3). The reactor was a Pyrex glass reaction vessel of 1 L of capacity (4).

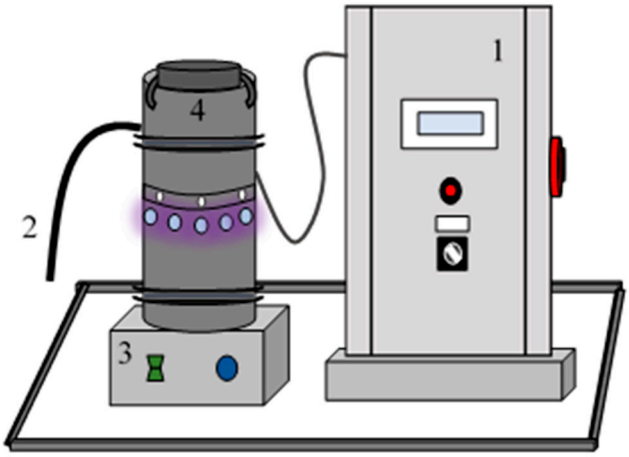

Figure 8. Experimental set up.

Thirty Light-Emitting Diodes (LEDs) (LED Enging LZ1-00UV00 (LED Enging Inc., San Jose, CA, USA)) with an emission wavelength of 365 nm were used as the light source. Ten strips with three LEDs surrounded the reaction vessel at a 3 cm distance from the reactor wall, as shown in Figure 9.

For each experiment, a synthetic solution of 30 mg/L of S-Metolachlor was prepared. NaOH and H_2SO_4 were used for pH adjustment. All the samples were filtered through a 0.45 µm nylon syringe filter (Filter-Lab, Filtros Anoia SA, Barcelona, Spain) before analysis.

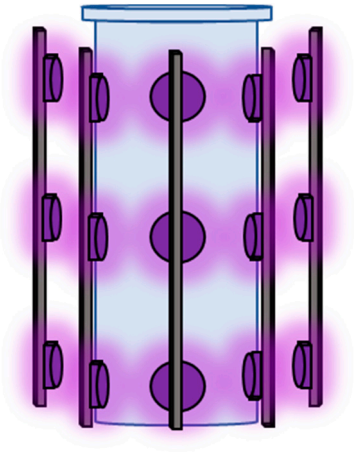

Figure 9. LED placement around the reactor.

3.3. Analytical Techniques

The MTLC concentration was measured in a High-Performance Liquid Chromatograph (HPLC) Agilent Series 1100 (Agilent Technologies, Santa Clara, CA, USA). The column was Zorbax Extend-C18 (5 µm, 3.0 × 150 mm) coupled to a photodiode array detector, both from Agilent Technologies. Distilled water and acetonitrile in a ratio of 60/40, respectively, were used as eluents with a flow rate of 0.75 mL/min.

The amount of chloride released during the experiments was determined by ion-exchange chromatography using an ICS-1100 ion chromatograph provided with autosampler AS40 (Dionex, Sunnyvale, CA, USA). The pH was quantified with an Edge pH Meter (Hanna Instruments, Woonsocket, Rhode Island, USA) previously calibrated with pH 4 and 7 standard solutions. All the experiments were conducted in duplicate at room temperature (25 °C).

3.4. Mathematical Model

For the evaluation of the radiation absorbed by the catalyst, the SFM model was employed, and LVRPA was calculated following Equation (3). The fundamentals of the mathematical model are detailed in the Supplementary Materials. This model considers that photon scattering could occur in the six directions of Cartesian coordinates [21].

$$\mathrm{LVRPA} = \frac{I_0}{\lambda_{\mathrm{Rcorr}} \times R_{\mathrm{corr}} \times (1-Y)} \times \left[\left(R_{\mathrm{corr}} - 1 + \sqrt{1-R_{\mathrm{corr}}^2} \right) \times e^{\frac{-Rp}{\lambda_{\mathrm{Rcorr}}}} + Y \times \left(R_{\mathrm{corr}} - 1 - \sqrt{1-R_{\mathrm{corr}}^2} \right) \times e^{\frac{Rp}{\lambda_{\mathrm{Rcorr}}}} \right] \quad (3)$$

I_0 is the incident light intensity in the wall of the photoreactor. R_{corr}, λ_{Rcorr} and Y are SFM parameters that were computed exclusively from the photocatalyst scattering albedo, reactor optical thickness and scattering phase function, respectively [29]. The independent variable R_p is the coordinate distance in the direction of the incident ray [30]. The incident radiation intensity was determined by Parker's actinometry based on the photochemical reduction of Fe(III) to Fe(II) from the ferrioxalate complex [45]. As LEDs were located at the same distance as the reactor wall and the light was homogeneously arranged, the value of I_0 was supposed constant. Finally, LVRPA distribution was assumed constant along the reactor height due to the homogeneity of the radiation field. Perfect mixing was considered in the batch reactor. The mathematical model integrated by Equations (1) and (S3)–(S10) from the Supplementary Material was solved with MATLAB (Mathworks). Once LVRPA had been estimated, the Overall Volumetric Rate of Photon Absorption (OVRPA) was determined, Equation (4). This equation is valid only for pseudoisotropic systems [32].

$$\mathrm{OVRPA} = \int_0^{\mathrm{V}} \mathrm{LVRPA}\ \mathrm{dV} \quad (4)$$

Finally, the kinetic model shown in Equation (1) was proposed to describe the removal of MTLC in the batch photocatalytic reactor including both kinetic and radiation parameters.

4. Conclusions

This work reports the kinetic study of the photocatalytic degradation of the pesticide S-Metolachlor with commercial TiO_2 P25 in a LED-assisted photoreactor including experimental and modeling perspectives. The experimental planning concluded with the best operating conditions in terms of degradation kinetics of the target pesticide: acidic conditions (pH 3) and 0.5 g/L of catalyst concentration.

The mathematical model accounting for photon absorption and the light field distribution in the photocatalytic LED reactor was then developed to be integrated into the kinetic model of the photocatalytic degradation of S-Metolachlor. Thus, the LVRPA calculation showed that the increase of catalyst concentration entailed greater photonic absorption on the reactor wall (0 m) but decreased inside the reactor until the minimum value was reached in the center of the reactor (0.04 m). The proposed model estimated the OVRPA. The maximum value was obtained for a catalyst concentration of 0.5 g/L. This result was in agreement with the experimental evidence.

Finally, the rate of S-Metolachlor photocatalytic degradation was described by a kinetic equation that accounted for the influence of radiation distribution inside the reactor as well as for the concentration of the target organic compound. The parameters that best fit the experimental data were m = 0.9 and n = 1.1, with a kinetic constant of 5.1×10^{-3} $(m^3)^{0.9}/W^{0.9}{\cdot}min{\cdot}mol^{0.1}$ (room temperature). However, second-order kinetic equations (m = 1 and n = 1) could also be useful for process design and control.

Supplementary Materials: The following are available online at https://www.mdpi.com/2073-4344/11/1/48/s1, Reactor Modelling; High-Performance Liquid Chromatography.

Author Contributions: Conceptualization, L.R., M.J.R. and I.O.; methodology, L.R., M.J.R., M.Á.M. and I.O.; formal analysis, L.R. and M.Á.M.; investigation, L.R. and M.J.R.; writing—original draft preparation, L.R. and M.J.R.; writing—review and editing L.R., M.J.R. and I.O.; supervision, M.J.R. and I.O.; project administration, M.J.R.; funding acquisition, M.J.R. and I.O. All authors have read and agreed to the published version of the manuscript.

Funding: This research was funded by the Spanish Ministry of Science, Innovation, and Universities (Grant Numbers: RTI2018-099407-B-I00 and RTI2018-093310-B-I00) (MCIU/AEI/FEDER, UE).

Conflicts of Interest: The authors declare no conflict of interest.

References

1. Dimou, A.D.; Sakkas, V.A.; Albanis, T.A. Metolachlor photodegradation study in aqueous media under natural and simulated solar irradiation. *J. Agric. Food Chem.* **2005**, *53*, 694–701. [CrossRef] [PubMed]
2. Jurado, A.; Vàzquez-Suñé, E.; Carrera, J.; de Alda, M.L.; Pujades, E.; Barceló, D. Emerging organic contaminants in groundwater in Spain: A review of sources, recent occurrence and fate in a European context. *Sci. Total Environ.* **2012**, *440*, 82–94. [CrossRef] [PubMed]
3. Orge, C.A.; Pereira, M.F.R.; Faria, J.L. Photocatalytic-assisted ozone degradation of metolachlor aqueous solution. *Chem. Eng. J.* **2017**, *318*, 247–253. [CrossRef]
4. Cavalier, T.C.; Lavy, T.L.; Mattice, J.D. Persistence of Selected Pesticides in Ground-Water Samples. *Ground Water* **1991**, *29*, 225–231. [CrossRef]
5. Environmental Protection Agency. Regulatory Determinations Support Document for Selected Contaminants from the Second Drinking Water Contaminant Candidate List (CCL 2). *Federal Register*, June 2008; pp. 1–29.
6. España. Real Decreto 817/2015, de 11 de septiembre, por el que se establecen los criterios de seguimiento y evaluación del estado de las aguas superficiales y las normas de calidad ambiental. *Boletín Oficial del Estado (BOE)*, 11 September 2015; pp. 38–40.
7. Otero, R.; López, M.I.; Esquivel, D.; Fernández, J.M.; Romero-Salguero, F.J. Removal of S-metolachlor herbicide from aqueous solutions by meso and microporous organosilica materials. *Microporous Mesoporous Mater.* **2019**, *278*, 35–43. [CrossRef]
8. Elsayed, O.F.; Maillard, E.; Vuilleumier, S.; Imfeld, G. Bacterial communities in batch and continuous-flow wetlands treating the herbicide S-metolachlor. *Sci. Total Environ.* **2014**, *499*, 327–335. [CrossRef] [PubMed]

9. Li, X.; Zhang, X.; Zhao, X.; Yu, B.; Weng, L.; Li, Y. Efficient Removal of Metolachlor and Bacterial Community of Biofilm in Bioelectrochemical Reactors. *Appl. Biochem. Biotechnol.* **2019**, *189*, 384–395. [CrossRef]
10. Sakkas, V.A.; Arabatzis, I.M.; Konstantinou, I.K.; Dimou, A.D.; Albanis, T.A.; Falaras, P. Metolachlor photocatalytic degradation using TiO_2 photocatalysts. *Appl. Catal. B Environ.* **2004**, *49*, 195–205. [CrossRef]
11. Guelfi, D.R.V.; Gozzi, F.; Machulek, A.; Sirés, I.; Brillas, E.; de Oliveira, S.C. Degradation of herbicide S-metolachlor by electrochemical AOPs using a boron-doped diamond anode. *Catal. Today* **2018**, *313*, 182–188. [CrossRef]
12. Dominguez, S.; Ribao, P.; Rivero, M.J.; Ortiz, I. Influence of radiation and TiO_2 concentration on the hydroxyl radicals generation in a photocatalytic LED reactor. Application to dodecylbenzenesulfonate degradation. *Appl. Catal. B Environ.* **2014**, *178*, 165–169. [CrossRef]
13. Escudero, C.J.; Iglesias, O.; Dominguez, S.; Rivero, M.J.; Ortiz, I. Performance of electrochemical oxidation and photocatalysis in terms of kinetics and energy consumption. New insights into the p-cresol degradation. *J. Environ. Manag.* **2017**, *195*, 117–124. [CrossRef] [PubMed]
14. Gomez-Herrero, E.; Tobajas, M.; Rodriguez, J.J.; Mohedano, A.F. Ionic liquids removal by sequential photocatalytic and biological oxidation. *J. Chem. Technol. Biotechnol.* **2020**, *95*, 1926–1935. [CrossRef]
15. Diaz, E.; Mohedano, A.F.; Casas, J.A.; Shalaby, C.; Eser, S.; Rodriguez, J.J. On the performance of Pd and Rh catalysts over different supports in the hydrodechlorination of the MCPA herbicide. *Appl. Catal. B Environ.* **2016**, *186*, 151–156. [CrossRef]
16. Dominguez, S.; Laso, J.; Margallo, M.; Aldaco, R.; Rivero, M.J.; Irabien, Á.; Ortiz, I. LCA of greywater management within a water circular economy restorative thinking framework. *Sci. Total Environ.* **2018**, *621*, 1047–1056. [CrossRef] [PubMed]
17. Tolosana-Moranchel, A.; Faraldos, M.; Bahamonde, A. Assessment of an intrinsic kinetic model for TiO_2-formic acid photodegradation using LEDs as a radiation source. *Catal. Sci. Technol.* **2020**, *10*, 6198–6211. [CrossRef]
18. Casado, C.; Timmers, R.; Sergejevs, A.; Clarke, C.T.; Allsopp DW, E.; Bowen, C.R.; van Grieken, R.; Marugán, J. Design and validation of a LED-based high intensity photocatalytic reactor for quantifying activity measurements. *Chem. Eng. J.* **2017**, *327*, 1043–1055. [CrossRef]
19. Acosta-Herazo, R.; Monterroza-Romero, J.; Mueses, M.Á.; Machuca-Martínez, F.; Puma, G.L. Coupling the Six Flux Absorption-Scattering Model to the Henyey-Greenstein scattering phase function: Evaluation and optimization of radiation absorption in solar heterogeneous photoreactors. *Chem. Eng. J.* **2016**, *302*, 86–96. [CrossRef]
20. Marugán, J.; van Grieken, R.; Cassano, A.E.; Alfano, O.M. Quantum efficiency of cyanide photooxidation with TiO_2/SiO_2 catalysts: Multivariate analysis by experimental design. *Catal. Today* **2007**, *129*, 143–151. [CrossRef]
21. Toepfer, B.; Gora, A.; Puma, G.L. Photocatalytic oxidation of multicomponent solutions of herbicides: Reaction kinetics analysis with explicit photon absorption effects. *Appl. Catal. B Environ.* **2006**, *68*, 171–180. [CrossRef]
22. Colina-Márquez, J.A.; López vásquez, A.F.; Machuca-martínez, F. Modelamiento de la reflexión solar directa en un colector parabólico compuesto (CPC) usando la técnica de 'ray-tracing'. *DYNA* **2010**, *77*, 132–140.
23. Puma, G.L.; Khor, J.N.; Brucato, A. Modeling of an annular photocatalytic reactor for water purification: Oxidation of pesticides. *Environ. Sci. Technol.* **2004**, *38*, 3737–3745. [CrossRef] [PubMed]
24. Brucato, A.; Rizzuti, L. Simplified Modeling of Radiant Fields in Heterogeneous Photoreactors. 2. Limiting 'Two-Flux' Model for the Case of Reflectance Greater Than Zero. *Ind. Eng. Chem. Res.* **1997**, *36*, 4748–4755. [CrossRef]
25. Romero, R.L.; Alfano, O.M.; Cassano, A.E. Cylindrical Photocatalytic Reactors. Radiation Absorption and Scattering Effects Produced by Suspended Fine Particles in an Annular Space. *Ind. Eng. Chem. Res.* **1997**, *36*, 3094–3109. [CrossRef]
26. Moreno, J.; Casado, C.; Marugán, J. Improved discrete ordinate method for accurate simulation radiation transport using solar and LED light sources. *Chem. Eng. Sci.* **2019**, *205*, 151–164. [CrossRef]
27. Puma, G.L. Modeling of Thin-Film Slurry Photocatalytic Reactors Affected by Radiation Scattering. *Environ. Sci. Technol.* **2003**, *37*, 5783–5791. [CrossRef] [PubMed]
28. Brucato, A.; Cassano, A.E.; Grisafi, F.; Montane, G.; Rizzuti, L.; Bella, G. Estimating Radiant Fields in Flat Heterogeniuos Photorreactors by the Six-Flux Modell. *AIChE J.* **2006**, *52*, 3882–3890. [CrossRef]
29. Mueses, M.A.; Machuca-Martinez, F.; Hernández-Ramirez, A.; Puma, G.L. Effective radiation field model to scattering–Absorption applied in heterogeneous photocatalytic reactors. *Chem. Eng. J.* **2015**, *279*, 442–451. [CrossRef]
30. Ochoa-Gutiérrez, K.S.; Tabares-Aguilar, E.; Mueses, M.Á.; Machuca-Martínez, F.; Puma, G.L. A Novel Prototype Offset Multi Tubular Photoreactor (OMTP) for solar photocatalytic degradation of water contaminants. *Chem. Eng. J.* **2018**, *341*, 628–638. [CrossRef]
31. Martín-Sómer, M.; Pablos, C.; van Grieken, R.; Marugán, J. Influence of light distribution on the performance of photocatalytic reactors: LED vs mercury lamps. *Appl. Catal. B Environ.* **2017**, *215*, 1–7. [CrossRef]
32. Mueses, M.A.; Machuca-Martinez, F.; Puma, G.L. Effective quantum yield and reaction rate model for evaluation of photocatalytic degradation of water contaminants in heterogeneous pilot-scale solar photoreactors. *Chem. Eng. J.* **2013**, *215–216*, 937–947. [CrossRef]
33. Sanchez, M.; Rivero, M.J.; Ortiz, I. Kinetics of dodecylbenzenesulphonate mineralisation by TiO_2 photocatalysis. *Appl. Catal. B Environ.* **2011**, *101*, 515–521. [CrossRef]
34. Rivero, M.J.; Ribao, P.; Gomez-Ruiz, B.; Urtiaga, A.; Ortiz, I. Comparative performance of TiO_2-rGO photocatalyst in the degradation of dichloroacetic and perfluorooctanoic acids. *Sep. Purif. Technol.* **2020**, *240*, 116637. [CrossRef]

35. Dominguez, S.; Rivero, M.J.; Gomez, P.; Ibañez, R.; Ortiz, I. Kinetic modeling and energy evaluation of sodium dodecylbenzene-sulfonate photocatalytic degradation in a new LED reactor. *J. Ind. Eng. Chem.* **2016**, *37*, 237–242. [CrossRef]
36. Carbajo, J.; Tolosana-Moranchel, A.; Casas, J.A.; Faraldos, M.; Bahamonde, A. Analysis of photoefficiency in TiO_2 aqueous suspensions: Effect of titania hydrodynamic particle size and catalyst loading on their optical properties. *Appl. Catal. B Environ.* **2018**, *221*, 1–8. [CrossRef]
37. Colina-Márquez, J.; MacHuca-Martínez, F.; Puma, G.L. Radiation absorption and optimization of solar photocatalytic reactors for environmental applications. *Environ. Sci. Technol.* **2010**, *44*, 5112–5120. [CrossRef] [PubMed]
38. Valencia, S.H.; Marín, J.M.; Restrepo, G.M. Efecto del pH en la Degradación Fotocatalítica de Materia Orgánica Natural. *Inf. Tecnol.* **2011**, *22*, 57–66. [CrossRef]
39. Richard, C.; Bengana, S. PH effect in the photocatalytic transformation of a phenyl-urea herbicide. *Chemosphere* **1996**, *33*, 635–641. [CrossRef]
40. Carrier, M.; Perol, N.; Herrmann, J.M.; Bordes, C.; Horikoshi, S.; Paisse, J.O.; Baudot, R.; Guillard, C. Kinetics and reactional pathway of Imazapyr photocatalytic degradation Influence of pH and metallic ions. *Appl. Catal. B Environ.* **2006**, *65*, 11–20. [CrossRef]
41. Casado, C.; Marugán, J.; Timmers, R.; Muñoz, M.; van Grieken, R. Comprehensive multiphysics modeling of photocatalytic processes by computational fluid dynamics based on intrinsic kinetic parameters determined in a differential photoreactor. *Chem. Eng. J.* **2017**, *310*, 368–380. [CrossRef]
42. Moreno-SanSegundo, J.; Casado, C.; Marugán, J. Enhanced numerical simulation of photocatalytic reactors with an improved solver for the radiative transfer equation. *Chem. Eng. J.* **2020**, *388*, 124183. [CrossRef]
43. Tolosana-Moranchel, A.; Pecharromán, C.; Faraldos, M.; Bahamonde, A. Strong effect of light scattering by distribution of TiO_2 particle aggregates on photocatalytic efficiency in aqueous suspensions. *Chem. Eng. J.* **2021**, 403. [CrossRef]
44. Tolosana-Moranchel, A.; Casas, J.A.; Carbajo, J.; Faraldos, M.; Bahamonde, A. Influence of TiO_2 optical parameters in a slurry photocatalytic reactor: Kinetic modelling. *Appl. Catal. B Environ.* **2017**, *200*, 164–173. [CrossRef]
45. Heath, H. A new sensitive chemical actinometer—II. Potassium ferrioxalate as a standard chemical actinometer. *Proc. R. Soc. Lond. Ser. A. Math. Phys. Sci.* **1956**, *235*, 518–536. [CrossRef]